CrossMark

Can large scale surface circulation changes modulate the sea surface warming pattern in the Tropical Indian Ocean?

S. Rahul[1] · C. Gnanaseelan[1]

© Springer-Verlag Berlin Heidelberg 2015

Abstract The increased rate of Tropical Indian Ocean (TIO) surface warming has gained a lot of attention in the recent years mainly due to its regional climatic impacts. The processes associated with this increased surface warming is highly complex and none of the mechanisms in the past studies could comprehend the important features associated with this warming such as the negative trends in surface net heat fluxes and the decreasing temperature trends at thermocline level. In this work we studied a previously unexplored aspect, the changes in large scale surface circulation pattern modulating the surface warming pattern over TIO. We use ocean reanalysis datasets and a suit of Ocean General Circulation Model (OGCM) experiments to address this problem. Both reanalysis and OGCM reveal strengthening large scale surface circulation pattern in the recent years. The most striking feature is the intensification of cyclonic gyre circulation around the thermocline ridge in the southwestern TIO. The surface circulation change in TIO is mainly associated with the surface wind changes and the geostrophic response to sea surface height decrease in the western/southwestern TIO. The surface wind trends closely correspond to SST warming pattern. The strengthening mean westerlies over the equatorial region are conducive to convergence in the central and divergence in the western equatorial Indian Ocean (IO) resulting central warming and western cooling. The resulting east west SST gradient further enhances the equatorial westerlies. This positive feedback mechanism supports strengthening of the observed SST trends in the equatorial Indian Ocean. The cooling induced by the enhanced upwelling in the west is compensated to a large extent by warming due to reduction in mixed layer depth, thereby keeping the surface temperature trends in the west to weak positive values. The OGCM experiments showed that the wind induced circulation changes redistribute the excess heat received in the western TIO to central and east thereby enhancing warming in the central equatorial IO. The increased surface warming in central TIO increases the latent heat loss, and keeps the net heat flux trends negative. Model sensitivity experiments reveal that the subsurface cooling at thermocline level in TIO is contributed by variability in Pacific via Indonesian Through Flow whereas the surface warming trend is mainly induced by the changes in the local forcing. The long term changes in IO Rossby waves are not induced by local atmospheric forcing but are forced by Pacific. The thermocline shoaling in the west is therefore amplified by the remote influence of Pacific via wave transmission through Indonesian archipelago.

Keywords Indian Ocean warming · Subsurface cooling · Local forcing · Remote forcing · Model sensitivity experiments

1 Introduction

The increasing trends in the global mean ocean heat content is mainly attributed to the global warming induced by anthropogenic activities (e.g. Barnett et al. 2005; Levitus 2005; Lyman et al. 2010). On a regional scale, the ocean warming is not uniform, and is influenced by the local climate and inherent coupled ocean-atmospheric modes of variability linked to the region (Xie et al. 2010). Understanding the processes responsible for the regional changes associated with the background warming is essential for

✉ C. Gnanaseelan
  seelan@tropmet.res.in

[1] Indian Institute of Tropical Meteorology, Pune 411008, India

understanding the observed climate change and for generating future projections.

Of all the tropical oceans, Tropical Indian Ocean (TIO) exhibits the strongest and robust warming with a basin wide warming signal (Alory et al. 2007; Du and Xie 2008; Deser et al. 2010). This surface warming has considerable influence on the climate of both local and remote regions (e.g. Giannini et al. 2003; Hoerling and Kumar 2003; Hoerling et al. 2004; Chung and Ramanathan 2006; Rao et al. 2010b; Williams and Funk 2011; Luo et al. 2012; Tokinaga et al. 2012). Besides its importance in modulating the climate of surrounding land mass, TIO warming has gained the attention of research community because of the complexity of the processes associated with the increased warming rate.

The heat content trends in World Ocean Database (WOD) indicate enhanced heat storage in southern Indian Ocean (IO) compared to north (Fig. S9 in Levitus et al. 2009). The vertical structure of IO temperature trends in Quality controlled Ocean thermal Archives (QuOTA) data also indicates that the warming is confined to the surface layers in TIO, but penetrates to deeper ocean in southern latitudes (south of 20°S) (Alory et al. 2007). A subsurface cooling trend is observed in central IO, around 100–200 m depths in QuOTA, which is also evident in WOD (Fig. 1 in Han et al. 2006). The signature of this subsurface cooling is visible in Sea Surface Height (SSH) trends, as decreasing SSH in southwestern TIO is evident in in situ and satellite observations (Han et al. 2010). Significant sea level increase is observed in tide gauge records over rest of the IO coast (Unnikrishnan and Shankar 2007; Han et al. 2010) consistent with the basin-wide warming. Ocean reanalysis datasets like SODA captures this thermocline signature very well [e.g. Vargas-Hernandez et al. (2015a)].

The basin-wide IO warming is well simulated by climate models (e.g. Barnett et al. 2005; Alory et al. 2007; Dong and Zhou 2014), but processes responsible for the warming are highly model dependent. Du and Xie (2008) showed that in Coupled Model Intercomparison Project Phase-three (CMIP3) models, IO warming is induced by the increase in downward longwave radiation due to Green House Gases (GHG), and is amplified by the water vapor and atmospheric feedbacks. The role of forcing by GHG and anthropogenic aerosols in IO temperature trends in models are pointed out by Cai et al. (2007, 2008) and recently by Dong and Zhou (2014). According to Alory et al. (2007) the deep reaching subtropical warming and equatorial subsurface cooling in CMIP3 models are related to a 0.5° southward shift in the subtropical IO gyre, driven by strengthening southern hemisphere westerly winds. Models also suggest that the remote influence from Pacific being transmitted to IO via Indonesian Through Flow (ITF) region (Alory et al. 2007; Schwarzkopf and Böning 2011; Trenary and Han 2013). Studies using forced ocean models suggest that the subsurface cooling in equatorial IO is mainly caused by surface wind changes, which resulted in enhanced Ekman

pumping velocity and thereby thermocline shoaling in the southwestern equatorial IO (Han et al. 2006, 2010; Trenary and Han 2008; Timmermann et al. 2010). A recent review of Indian Ocean decadal variability by Han et al. (2014) further substantiates the role of wind induced oceanic response in decadal SSH/thermocline variability. Vargas-Hernandez et al. (2015b) showed that westward propagating salinity anomalies also can modulate the SSH variability in decadal and longer time scales over southern TIO. Many coupled climate models which successfully simulated the surface warming, could not reproduce this thermocline response (e.g. Alory and Meyers 2009; Dong et al. 2013).

Many studies have proposed possible mechanisms for the increased warming rate of TIO. Most of them concentrated on summertime warming, which is apparently the season in which warming is more prominent. Li et al. (2012) attributed the warming of TIO during summer time to asymmetry in ENSO variability. They showed that the decaying phase of El Nino, which induces warming in western TIO, has been delayed from spring to early summer in recent decades, while the seasonal timing of La Nina decay phase remains in spring season. Roxy et al. (2014) showed that the long term warming trend over the western Indian Ocean during summer is a result of asymmetry in El Nino–La Nina teleconnection (in the initial phase of ENSO). They pointed out that the increasing frequency of ENSO events in recent years also contributes to the warming. Swapna et al. (2013) suggested that the weakening summer monsoon circulation can enhance the equatorial SST trends in summer months. However the mechanisms responsible for the SST trends in the annual picture need careful scrutiny.

Though SST trends show most significant increase over TIO, the net heat flux into the ocean shows a decreasing trend over the entire TIO basin (Schott et al. 2009). Rahul and Gnanaseelan (2013) analyzed different heat flux products and showed that all the heat flux products show decreasing net heat flux over central TIO, and is mainly caused by increased latent heat loss as a response to increased SST and wind strength. Previous studies which addressed the issue of TIO warming, could not explain these two major dilemmas, the subsurface cooling at thermocline level and the negative trend in net heat flux. In this study we explore the role of surface ocean circulation changes in TIO warming and establish a possible mechanism which can explain these uncertainties.

2 Data and methods

2.1 Datasets

Ocean reanalysis datasets are used to understand the long term changes in the basin scale circulation pattern. We use

datasets from two different sources, European Centre for Medium-range Weather Forecasts (ECMWF) Ocean Reanalysis System 4 (ORAS4) and Simple Ocean Data Assimilation (SODA). Though uncertainties are relatively more prior to 1970s due to sparse observations, persistent changing trends throughout the study period (especially during the recent decades) can be considered as a robust signal. A brief description of both the products is provided for ready reference.

The ORAS4 dataset is available from 1958 to near present (ftp://ftp.icdc.zmaw.de/EASYInit/ORA-S4/). Detailed description and evaluation of ORAS4 assimilation system is provided in Balmaseda et al. (2013). Surface heat and momentum fluxes from ERA-40 reanalysis (from 1958 to December 1988) and from ERA-Interim reanalysis (from January 1989 to December 2009) are used to force OGCM. The heat flux variability is relatively unimportant in surface heat gain, as a strong relaxation to the observed SST is applied as a flux correction. Temperature and salinity profiles from quality controlled EN3v2a dataset (Ingleby et al. 2007) and along track altimeter-derived sea-level anomalies from AVISO (Archiving, Validation and Interpretation of Satellite Oceanographic data, http://www.aviso.ocean-obs.com/) are assimilated to model derived ocean state. As Boussinesq approximation is made in the OGCM, the correction for global steric sea level rise is provided as spatially uniform fresh water flux.

SODA (Carton and Giese 2008) version 2.1.6 used in this study is available for the period from 1958 to 2008. The OGCM used in this version is the Parallel Ocean Program (POP 2.1), an eddy permitting model with an average $0.25° × 0.4°$ horizontal resolution and 40 vertical levels. Surface winds are from ERA40 reanalysis up to 2002 and Quikscat scatterometer winds from 2002 to 2008. The temperature and salinity profiles from World Ocean database (WOD09) (http://www.nodc.noaa.gov/OC5/WOD/pr_wod.html) are assimilated to model derived ocean state. Ungridded nighttime NOAA/NASA Advanced Very High Resolution Radiometer (AVHRR) SST data is used to update surface temperature. Use of nighttime retrievals reduces the problem of correcting for skin temperature effects due to daytime heating.

The surface wind forcing of corresponding datasets are used for analysis. The historical SST reconstructions provided by met office Hadley centre [HadISST, (Rayner et al. 2003)] and NOAA extended reconstructed SST [ERSST v3b, (Smith et al. 2008)] are also used.

2.2 Methodology

The annual mean values (averaged from March to the following February) of different parameters are used in the analysis. Anomalies represent deviation of annual mean from long term mean. Helmholtz decomposition of ocean currents is performed to derive the stream function and velocity potential for understanding large scale circulation pattern. The methodology proposed by Watterson (2001) is used to deal with irregular coastal boundary conditions while decomposing ocean currents to rotational and divergent components.

2.3 OGCM and experiment details

2.3.1 OGCM

The Geophysical Fluid Dynamics Laboratory (GFDL), Modular Ocean Model version 4 (MOM4p1) (Griffies et al. 2004) is used for this study. The model is a fully complex ocean-ice model designed primarily as a tool for studying the ocean climate system (Griffies et al. 2005). Model is hydrostatic and non Boussinesq, with pressure based vertical coordinates. Model is configured for the Indo-Pacific basin (30°E–70°W, 60°S–30°N), with 0.25° uniform horizontal resolution. On the northern and southern boundaries, sponge layer of 2.5° thickness is used, where temperature and salinity is relaxed to climatological values of World Ocean Atlas 2009. There are 50 vertical levels with 10 m resolution in first 250 m. Realistic bottom topography from Sindhu et al. (2007) bathymetry data (based on NOAA-ETOPO5, but improved shelf bathymetry for the Indian Ocean region) is provided. Topography is filtered to remove small scale grid noises, without disturbing the original geometry. The very fine channels in Indonesian ITF region either became shallower or got closed when topography is interpolated to models native grid. So we artificially modified the width and depth of the narrow channels in ITF region as well as in the openings of Red sea and Persian Gulf, to allow reasonable flow into IO basin.

The K-profile vertical mixing parameterization (Large et al. 1994) is used for surface mixing. The horizontal viscosity is parameterized using Biharmonic Smagorinsky scheme (Griffies and Hallberg 2000). Fox-Kemper et al. (2008) submesoscale parameterization and Simmons et al. (2004) parameterization for tidal mixing are also employed. Manizza et al. (2005) scheme for shortwave penetration is applied, using the Seasonal climatology of chlorophyll based on NASA SeaWIFS satellite measurements.

2.3.2 Experiments

The Coordinated Ocean-ice Reference Experiments (CORE) surface forcing datasets for global ocean-ice modeling (Large and Yeager 2008), is used to force the OGCM for this study. Technical details of version 2 of CORE dataset is available at ftp://go-essp.gfdl.noaa.gov/1p/nnz/COREv2/doc/release_notesV2_10Feb2011.pdf. In the

model, turbulent heat fluxes are derived from the bulk formula using the model SST and the 10 m atmospheric fields in CORE forcing. Radiative heating is provided by shortwave and incoming long wave fluxes.

The model is spun up with CORE Normal Year Forcing (NYF) for 100 years. From there model is forced with CORE Inter Annual Forcing (IAF) from 1958 to 2008. This experiment is here after referred as CONTROL. To isolate the role of surface wind and heat fluxes in IO warming trends, two experiments are designed. One with climatological winds i.e. winds in NYF applied repeatedly each year, and interannual heat fluxes (named as CLIM-WIND). The other one is with climatological heat flux and interannual winds (named as CLIM-FLUX). The surface heat and salt fluxes are modulated every time the wind speed is changed in the model, as the evaporation and corresponding latent heat flux depend upon wind magnitude. So, the daily net heat and salt fluxes of the CONTROL are used to force the model in CLIM-WIND experiment, so that irrespective of wind changes model gets same heat and fresh water forcing as in CONTROL. A daily climatology of CONTROL net heat flux is used in CLIM-FLUX, which prevents the net heat flux to vary inter-annually with the wind magnitude. One more experiment is done where the model is started from same state as in CONTROL, but forced with normal year forcing for the same time span of CONTROL (named as CLIM). The effect of interannualy varying forcing is isolated by subtracting CLIM from other experiments to remove drifts in the model's mean state.

To study the role of remote forcing from Pacific via Indonesian archipelago, we modulated the forcing fields over Pacific and Indian Ocean in separate experiments. In CLIM-PO experiment, the Pacific Ocean is forced with NYF, while IO is forced with IAF. Another experiment is carried out with NYF over IO and IAF in Pacific (CLIM-IO).

3 Pattern of SST trends and surface wind response

The SST trends in two historical SST reconstructions as well as in the ocean reanalysis data sets for the period 1958–2008 is shown in Fig. 1. SST trends show weaker warming pattern in the western equatorial region compared to central and eastern parts in all the data sets for this time period. The difference in SST averaged over central and western region (Fig. 1e) indicates an increasing west to east SST gradient along the equatorial region from 1958 to 2008. The argument that the western equatorial IO is warming faster than the central and eastern parts made by Roxy et al. (2014) is the case when the trend is computed from 1900 onwards, as the period of 1900–1950 shows increased

surface warming in the west (figure not shown). The west to east gradient also shows decreasing tendency from 1900 to 1958. The trend pattern of reanalysis data sets agree well with that of SST data sets. Particularly, SODA shows the weakest trend in the western equatorial region.

The response of this SST trend pattern can be identified in surface wind trends. The trend vectors of annual mean wind stress field (used as the forcing for respective reanalysis data sets) is shown in Fig. 1c, d. Swapna et al. (2013) reported that radiosonde observations at Bombay (a station in the west coast of India) indicates weakening of surface zonal winds. Mishra et al. (2012) showed that southward deflection of moist, westerly monsoon flow from the Arabian Sea resulted in a reduced flux of moisture towards Indian subcontinent. Such response is clearly evident in the trend pattern shown in Fig. 1c, d. The trend vectors converged where the SST trends are maximum, i.e. over the central equatorial IO and central Arabian Sea.

Since the annual mean winds north of 5°S is an average of seasonally reversing winds, we computed the wind stress trends and SST trends for the four seasons separately to see whether the convergence of winds towards equatorial region is a seasonal response (figure not shown). In all seasons the surface warming trend is maximum over central IO. The strengthening of easterly trade winds south of equator and westerly wind along central and eastern equatorial IO are apparent in all the seasons except in winter. In all the seasons, the trend vectors point away from the Indian subcontinent towards the oceanic region, which indicates weakening the moisture transport towards land. The strengthening cross equatorial winds along the western boundary during JJAS is apparent, but is similar to the trends in annual mean flow, with reduced inland flow. Weakening of meridional SST gradient along 60°E–100°E latitude band over the northern IO in summer monsoon months was reported by Chung and Ramanathan (2006). The relatively low rate of warming in the western equatorial IO (west of 60°E) as well as northern Arabian Sea (north of 20°N), compared to the central Arabian Sea explains the trend pattern of winds in summer season. The trend vectors south of 15°N over Arabian Sea indicate strengthening south-westerlies, while trend vectors north of 15°N indicate reduced flow towards land. Thus the reduction in meridional SST gradient and strengthening of zonal SST gradient assists the winds over central Arabian Sea to turn towards warmer equatorial region. This in turn enhances the equatorial westerlies.

4 Surface ocean circulation response to changing wind pattern

To visualize the mean surface circulation response to changing wind pattern over TIO, the stream functions
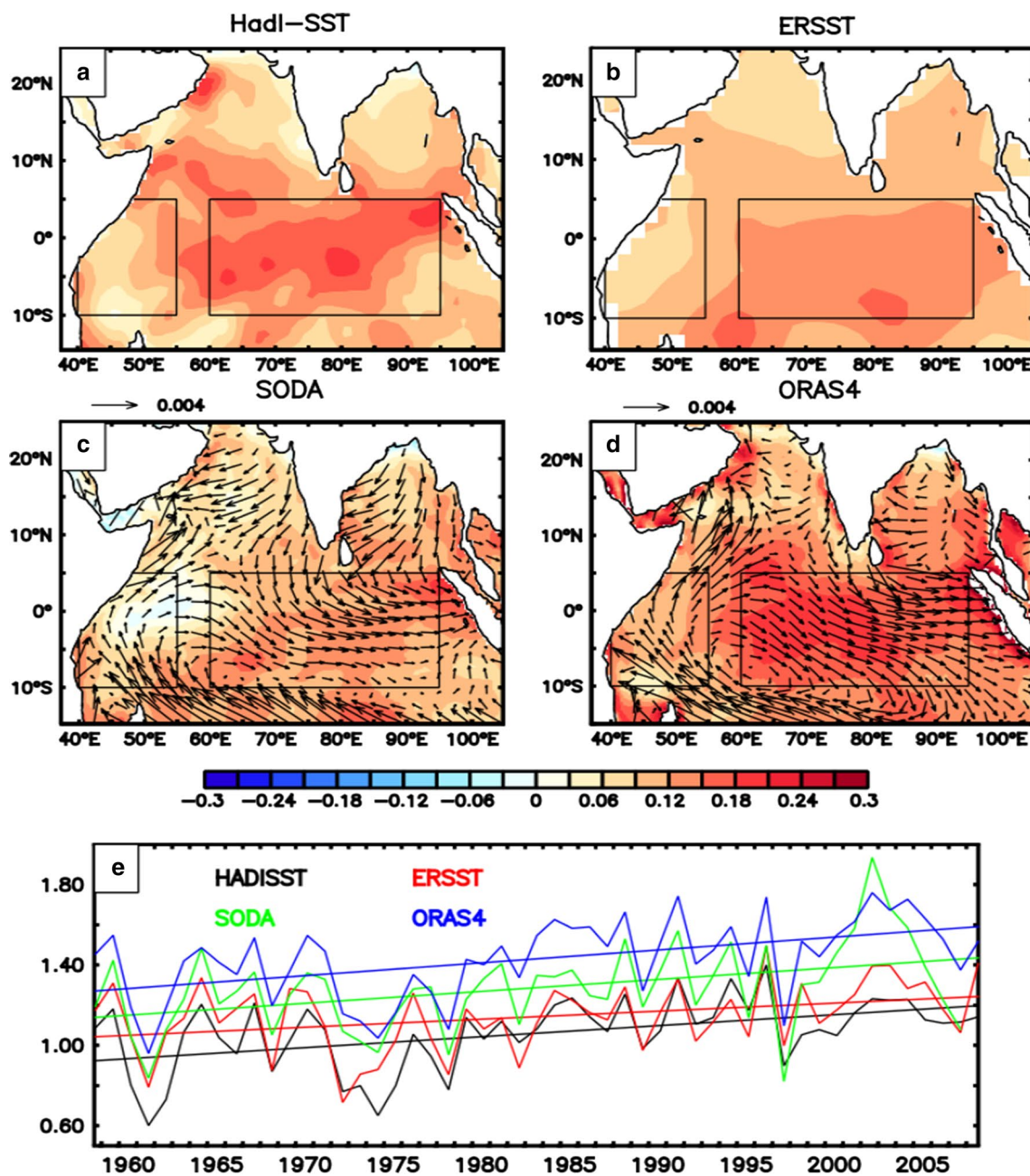
Fig. 1 *Shaded* are SST trend ($^{\circ}$C/decade) in **a** HadISST, **b** ERSST, **c** SODA and **d** ORAS4 from 1958 to 2008. Trends in corresponding wind stress forcing (Wm^{-2}/decade) of SODA and ORAS4 are over-laid as vectors in **c** and **d**. The difference between SST averaged over central and western boxes are shown in **e** (central minus western box. *Boxes* are marked in *top panels*)

derived from the annual mean surface currents (first 50 m) in the reanalysis datasets are averaged for the earlier (1958–1967) and recent (1999–2008) decades (Fig. 2). The mean surface circulation features of TIO in different seasons are intensively discussed in several studies (Shenoi et al. 1999; Schott and McCreary 2001; Schott et al. 2009). The annual mean circulation pattern is featured by a clockwise gyre in the thermocline ridge region of southwestern equatorial IO [here after referred as Thermocline Ridge Gyre (TRG)].

The strengthening of TRG circulation in recent decade is clearly visible in both datasets. Weak north–south flow along the equator in the first decade has been replaced by strong eastward flow in recent years which is extending southwards (up to about 5° from equator). The clockwise circulation around the thermocline ridge has further inten-sified and extended eastwards. The SSH trends in both data sets (see Fig. 3a, b) clearly show the decrease of SSH in the western and central equatorial IO. The intensification
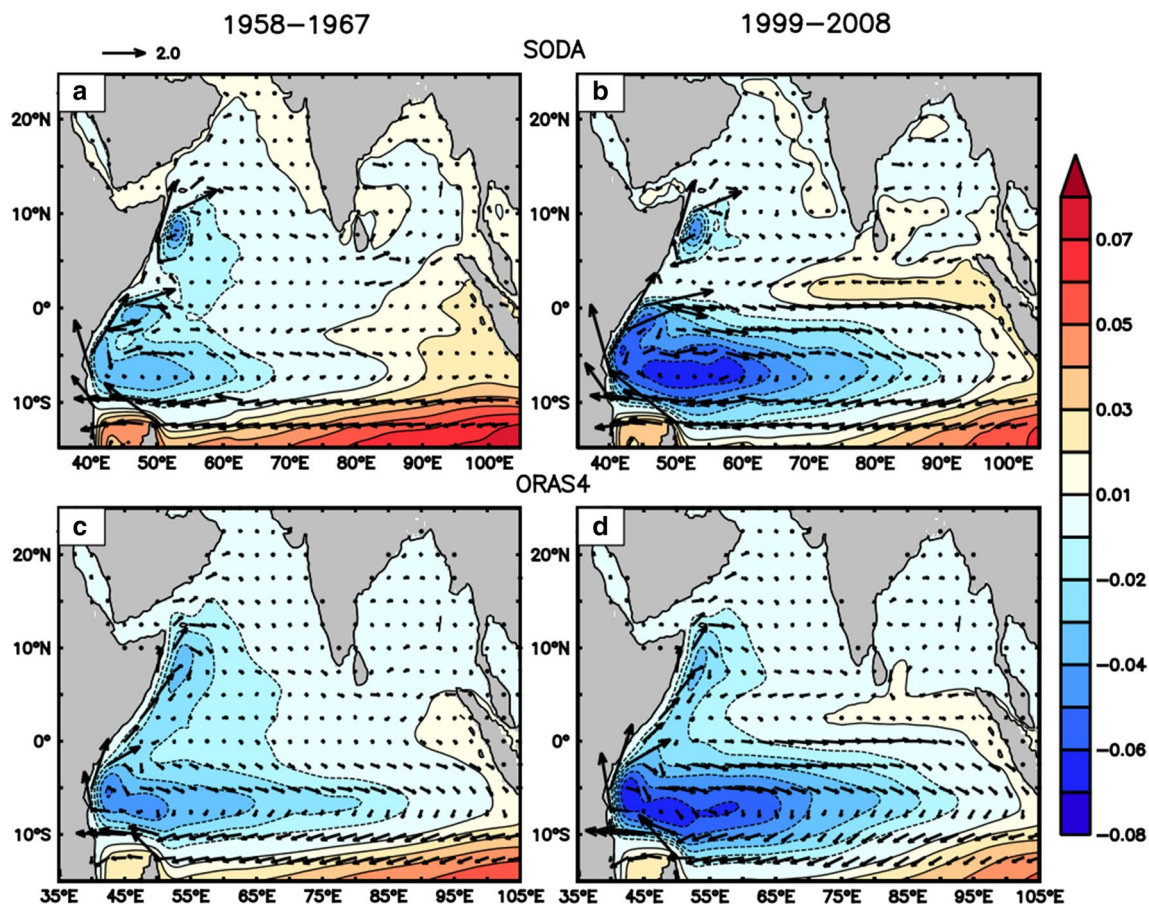
Fig. 2 Mean stream function (Sv, *shaded*) and corresponding rotational component (in 10^4 m²/s, vectors) of upper 50 m volume fluxes in SODA: **a** from 1958 to 1967, **b** from 1999 to 2008, **c**, **d** are same as **a** and **b** but for ORAS4

and eastward extension of zone of SSH minima indicate that increased gyre strength is a geostrophic response of decreased SSH/thermocline depth in the western equatorial IO. The mean velocity potential for first and last decades of the study period is shown in Fig. 4. Both data sets show divergence in the western equatorial region and convergence in the southeast, which is consistent with the known overturning circulation pattern in TIO (subduction in the southeast and upwelling in the western equatorial region). Over the recent decade the divergence in the western equatorial region as well as the convergence along central and eastern equatorial IO has increased considerably.

To identify the pattern of long term variability in TIO circulation we did Empirical Orthogonal Function (EOF) analysis of the stream function and velocity potential. A seven year running mean is applied to the anomalies before computing EOF to isolate long term variability. The first EOF mode and the corresponding Principal Component (PC) of stream function derived from both SODA and ORAS4 are shown in Fig. 5. The rotational currents derived from the EOF pattern are overlaid as vectors. First mode explains

89 % (78 %) of the total variability in SODA (ORAS4). The EOF pattern shows asymmetric circulation anomalies across the equator, with a clockwise circulation to the south and anticlockwise to the north. The PC time series shows a positive trend indicating strengthening of this circulation pattern over last half century. The circulation anomalies south of the equator in EOF clearly demonstrate the strengthening of the TRG circulation. The EOF pattern indicates convergence and eastward movement of water along the equator. The clockwise (anticlockwise) circulation anomalies in south (north) of equator are associated with upwelling and low SSH at the circulation centers (see Fig. 3a, b). The increasing trend in circulation suggests strengthening of upwelling at the center of the gyre structures. The increasing convergence towards equatorial region is well evident in similar EOF analysis of the velocity potential (Fig. 6). The dominant mode of variability of velocity potential represents divergence in the western and convergence in the central and eastern equatorial region. Here too the positive trend in PC indicates increasing convergence in the eastern and central equatorial IO and increasing divergence in the west.
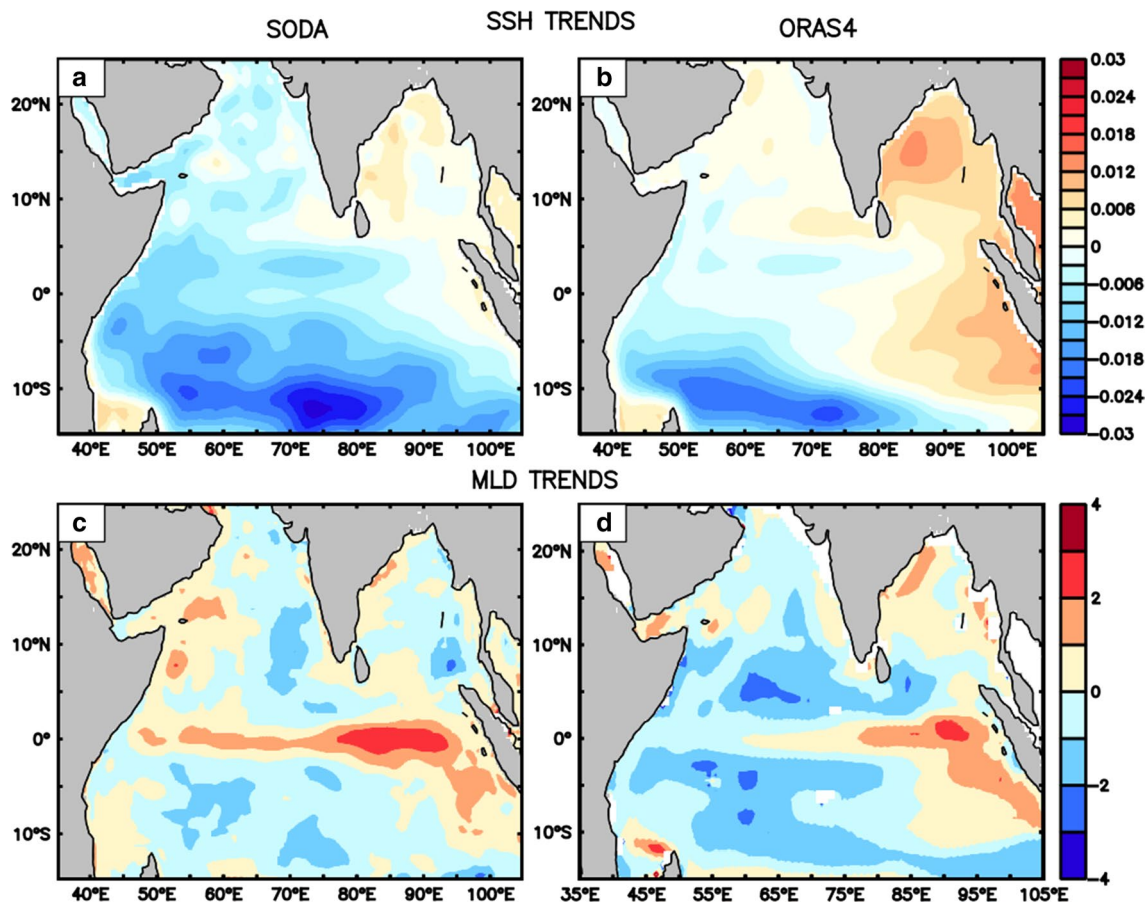
Fig. 3 SSH trends (metre/decade) in **a** SODA, **b** ORAS4. MLD trends (metre/decade) in **c** SODA, **d** ORAS4

The changing wind and ocean circulation pattern near the equator can influence the SST warming pattern, as the near equatorial westerly anomalies can induce convergence of warm water along the equator and increase sea level there which can then be propagated eastward as equatorial Kelvin waves. These waves after reaching the eastern boundary propagate northward as coastal Kelvin waves (Rao et al. 2010a; Sreenivas et al. 2012). Nidheesh et al. (2013) reported connection between equatorial Indian Ocean and Bay of Bengal (BOB) SSH anomalies through such mechanism at decadal time scales. At the same time, the sea surface low due to wind stress curl on both sides of equator can propagate westward as off equatorial upwelling Rossby waves, enhancing the upwelling and surface cooling over the west. Note that the SSH do display a decreasing trend over off equatorial central IO (Fig. 3). The first EOF pattern of stream function also indicates strengthening of cyclonic circulation in off equatorial region. The intensifying easterly trade winds south of equator as well as westerlies along the equator do favor intensification of divergence, Ekman pumping and cooling in the western and south-western equatorial IO. At the same time

strengthening of equatorial westerlies favor convergence of warm water in the eastern and central equatorial IO. This can increase the east–west SST gradient, which can further enhance the equatorial westerlies.

From the above analysis, it is clear that both surface winds and ocean circulation changes favor cooling of western equatorial IO. But SST observations indicate a weak positive trend over western equatorial IO. The western equatorial IO is the region where maximum heat input takes place over TIO (figure not shown). The upwelling zones in ocean are the regions were ocean intakes maximum heat, as relatively cooler surface temperature means more insolation (cloud free conditions) and lesser evaporative heat loss. The advection of heat by prevailing currents and the upwelling of colder water from the deeper oceans maintain the heat balance in such regions. The turbulent mixing in the ocean distributes the heat received in the surface up to Mixed Layer Depth (MLD). The MLD is a key factor in SST distribution as it determines the depth up to which the surface heat is mixed. We computed the MLD from the two reanalysis datasets to find out its long term trends.
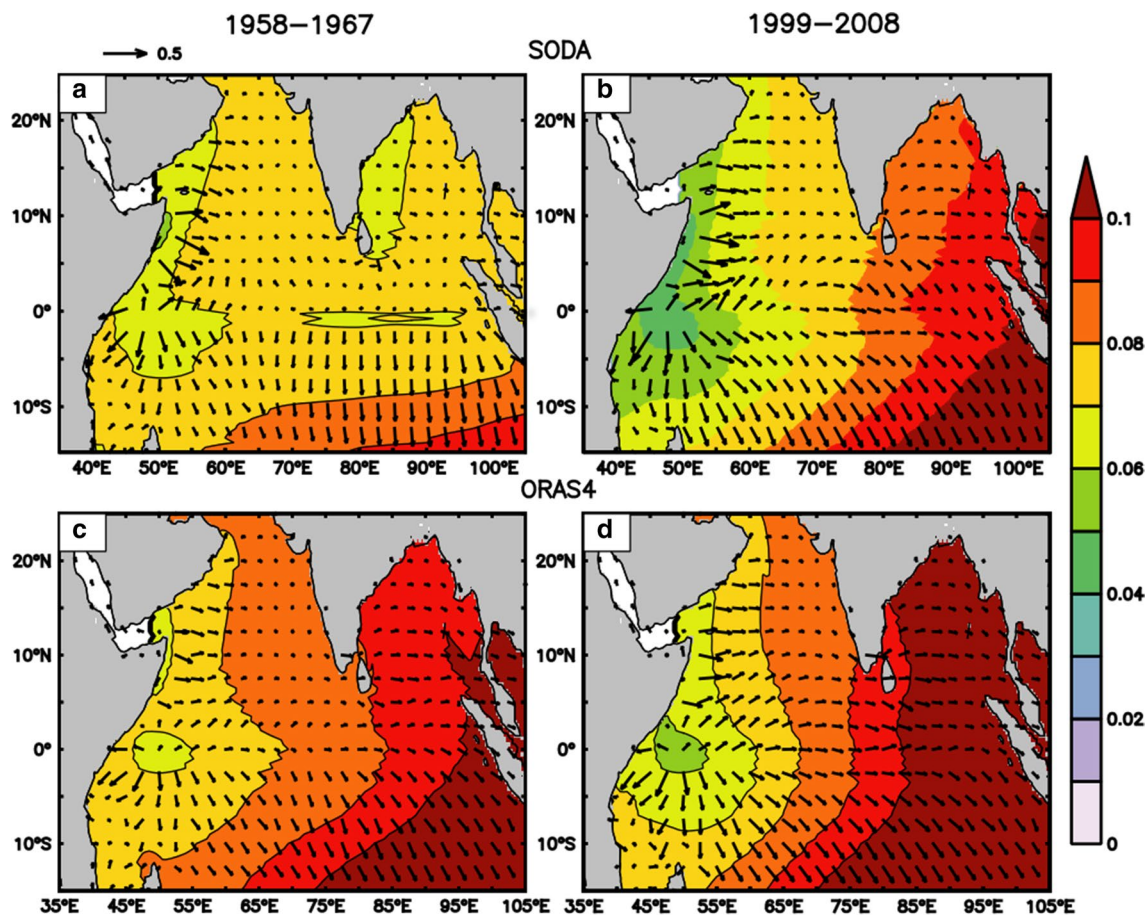
Fig. 4 Similar to Fig. 2 but for velocity potential and corresponding divergent component (in 10^4 m^2/s)

MLD is defined as the depth at which the density change corresponds to 0.8 °C change in surface temperature, for the given surface salinity (Kara et al. 2000). The trend in the annual mean MLD is shown in Fig. 3c, d, which clearly shows decreasing trend in most of TIO region, except for central and eastern equatorial regions and over coastal Bay of Bengal and Arabian sea. The decrease in MLD gives a possible explanation for the warming of western and southwestern equatorial IO where the ocean dynamics favors cooling. The decreasing subsurface (below MLD) temperature, due to dynamically induced enhanced upwelling resulted in an increased surface stratification and reduced MLD, particularly in the west where surface receives maximum heat. The heat received in the upper ocean is retained within a relatively shallower layer keeping the surface temperature trends more or less constant. The increase in surface winds along the west should enhance turbulent mixing, but the MLD trends indicate that the enhanced winds could not overcome the stratification generated by the shoaling of thermocline in the western equatorial IO.

5 OGCM simulations

The above discussions clearly support the role of ocean dynamics in modulating TIO surface warming pattern. A key limitation of reanalysis products is their inability to quantify the role of circulation in temperature changes, as data assimilation results in heat sources or sinks in the system. The OGCM simulations, where heat and momentum budgets are strictly closed, are instead used to isolate the role of dynamic versus thermodynamic forcing on IO warming.

5.1 CONTROL experiment

The SST, SSH and MLD trend in CONTROL experiment is shown in Fig. 7. The SST in the control experiment displays basin wide increasing trend with maximum warming in central and eastern TIO and very weak values in the western TIO near the Somali coast. The SSH is increasing over the central and eastern equatorial region and along the Indian coast. This pattern is consistent with reanalysis
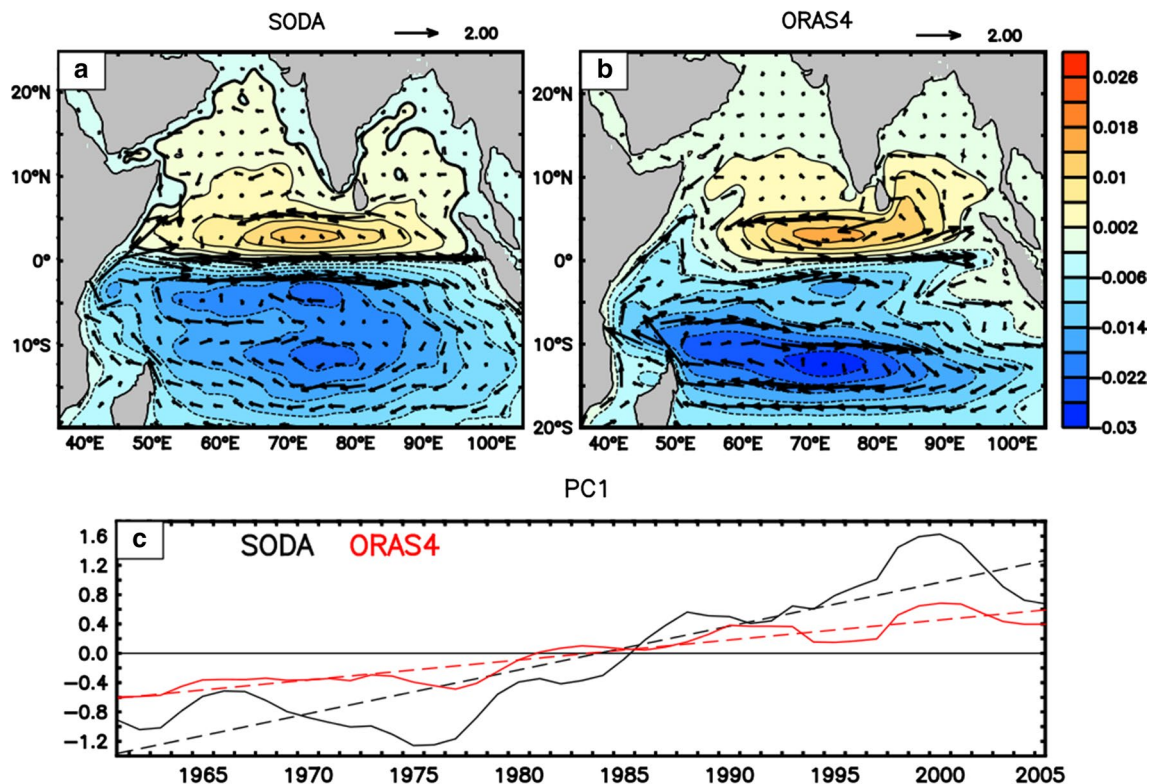
Fig. 5 The first EOF pattern of stream function in **a** SODA, **b** ORAS4, after applying a 7 year running mean. The currents derived from the corresponding eigenvectors (in 10^{-3} m²/s) are overlaid. The corresponding PC of SODA (*black*) and ORAS4 (*red*) are plotted at *bottom*. The *dashed lines* represent least square fit of the respective time series

datasets and observations (e.g. Han et al. 2010) where they show evidence of SSH increase along the Indian coast and eastern equatorial IO from tide gauge observations. The model MLD shows decreasing trend in the western equatorial region, southern Arabian Sea (AS) and central BOB while deepening MLD is visible in central equatorial region. The similarity between SSH and MLD trends in model suggests that surface warming and dynamically induced subsurface cooling can increase surface stratification, which results in shoaling of mixed layer in the western and off equatorial IO.

The mean stream function for the first and last decades in the CONTROL experiment is shown in Fig. 8. The intensification of TRG is captured by the OGCM. In the OGCM, the first decade (1958–1967) itself displays eastward currents along the equator and strong southward return flow along the eastern equatorial regions. Both these features have strengthened in recent decade, without any noticeable change in the spatial circulation pattern. The OGCM is forced with CORE winds, based on National Center for Environmental Prediction/National Center for Atmospheric Research (NCEP–NCAR) while reanalysis datasets were forced with ERA winds. Like surface forcing of reanalysis datasets, the CORE wind forcing also indicates reduced

winds towards Indian peninsula and convergence towards equator (figure not shown). But strengthening of cross equatorial southwesterly winds along western boundary is not so evident in CORE winds. Instead trend vectors are mostly eastward along the equator.

5.2 Sensitivity experiments

5.2.1 Dynamic v/s thermodynamic forcing

Sensitivity experiments are carried out by controlling the surface forcing parameters to isolate the role of ocean dynamics in surface warming of TIO in OGCM. The role of ocean dynamics is fully isolated in NHF-CLIM experiment (Fig. 9), where surface is forced with interannual wind forcing and daily climatology of net heat flux from CONTROL experiment. The NHF-CLIM trends indicate that the changes in surface wind forcing alone results in cooling of the TIO surface. The cooling trend is strongest in the western TIO north of equator. This supports the argument that the wind induced circulation changes can reduce the warming trend in western equatorial IO.

The SST trends in WIND-CLIM (Fig. 10, climatological winds and interannual heat fluxes) show surface warming
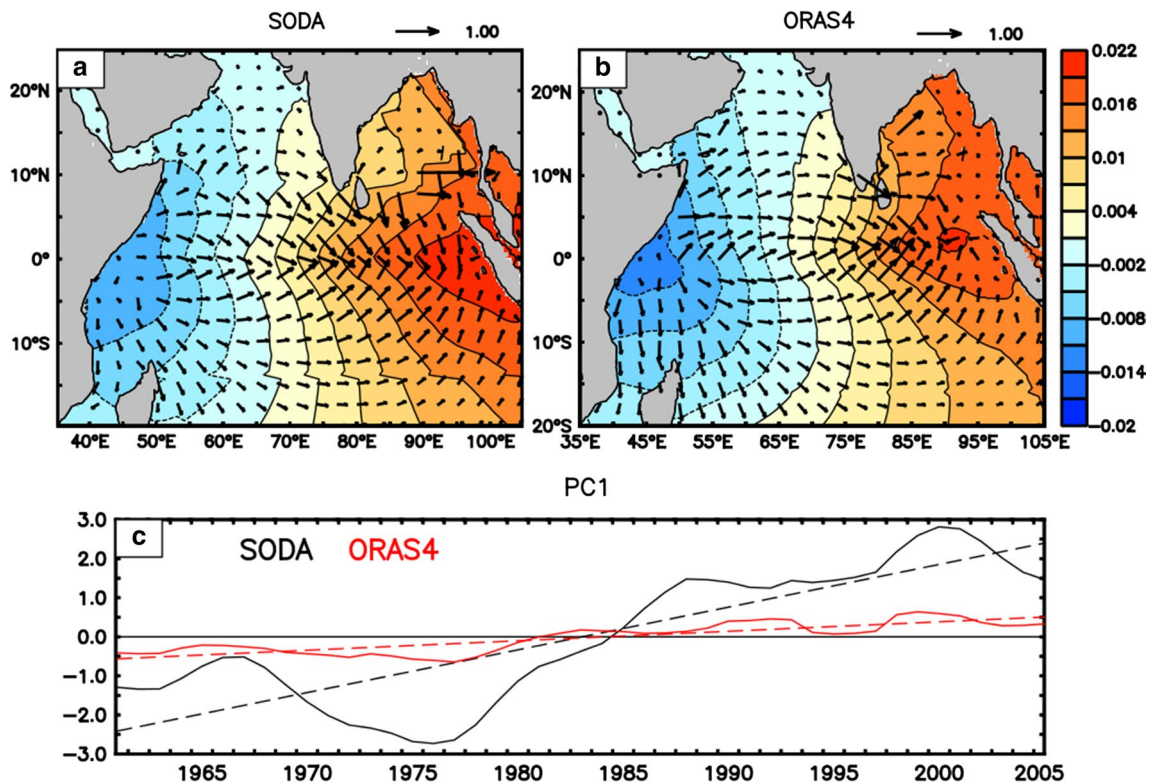
Fig. 6 Same as Fig. 5, but for velocity potential

in the western and central TIO, with maximum warming in the western equatorial IO. As pointed out earlier, the western equatorial IO is a region where IO gains maximum heat. The WIND-CLIM experiment proves that in the absence of wind induced circulation changes, heat is building up in western and central IO. In CONTROL experiment, the strengthened surface circulation redistributes this excess heat to the central and eastern TIO. The negative SST trends in NHF-CLIM experiment prove that in the absence of this heat flux changes, the strengthening ocean circulation tends to cool the surface.

The SSH trend in the NHF-CLIM shows shoaling SSH in the western equatorial IO similar to the CONTROL. The WIND-CLIM experiment does not display such trends indicating that the SSH trends in the west are mainly forced by wind changes. In NHF-CLIM, the deepening of SSH in the central IO (which is visible in CONTROL) is not well evident as in CONTROL, though relatively weaker SSH trends are visible. At the same time the MLD trend in the NHF-CLIM shows deepening MLD in central IO. The increase in MLD results in cooler SST, as available heat is distributed to deeper water column. But in the CONTROL experiment, the surface water converging may be warmer because of increased heat gain at the west, which contributes to the positive SST trend in the central and eastern IO. The decrease of MLD in western equatorial region is

evident in both NHF-CLIM and the WIND-CLIM experiments, confirming that that the surface heat flux forcing and wind induced ocean response, both act together to increase stratification and shoal MLD in the western equatorial IO. The sensitivity experiments clearly indicate that the surface wind forcing changes and the associated coupled interactions play a major role in the distribution of the excess heat received in the TIO. The observed pattern of SST trend is highly influenced by the oceanic response to the surface wind forcing.

5.2.2 Remote forcing from Pacific via Indonesian Archipelago

The influence of remote forcing from Pacific via ITF region is isolated using the two sensitivity experiments, CLIM-PO (inter annual forcing only over Indian Ocean) and CLIM-IO (inter annual forcing only over Pacific). The CONTROL and CLIM-PO experiment show almost similar SST trend pattern (figure not shown), suggesting that the surface warming of TIO is mainly induced by local forcing. It is important to note here that the local atmospheric forcing includes the remote forcing from Pacific via atmospheric teleconnections. The experiment shows that Pacific Ocean influence though oceanic pathways has negligible role on long term surface warming trends.
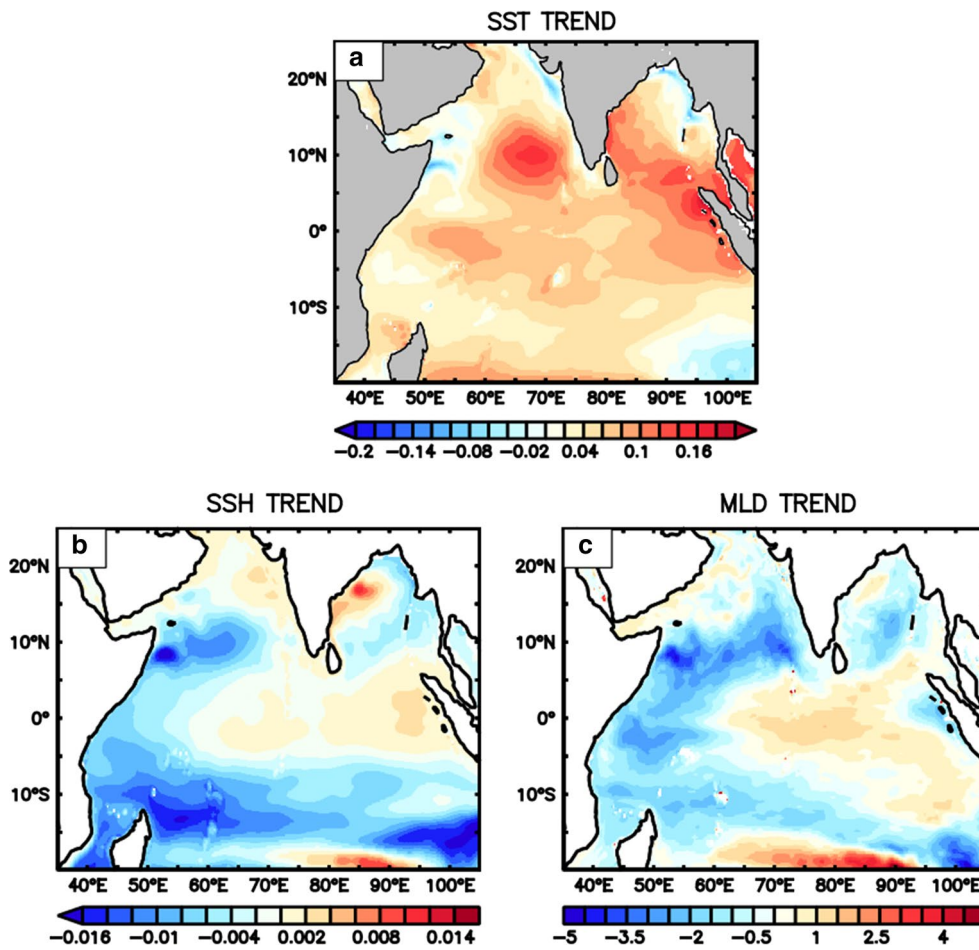
Fig. 7 **a** SST trends (°C/decade), **b** SSH trends (metre/decade), **c** MLD trend (metre/decade) in CONTROL experiment (1958–2008)
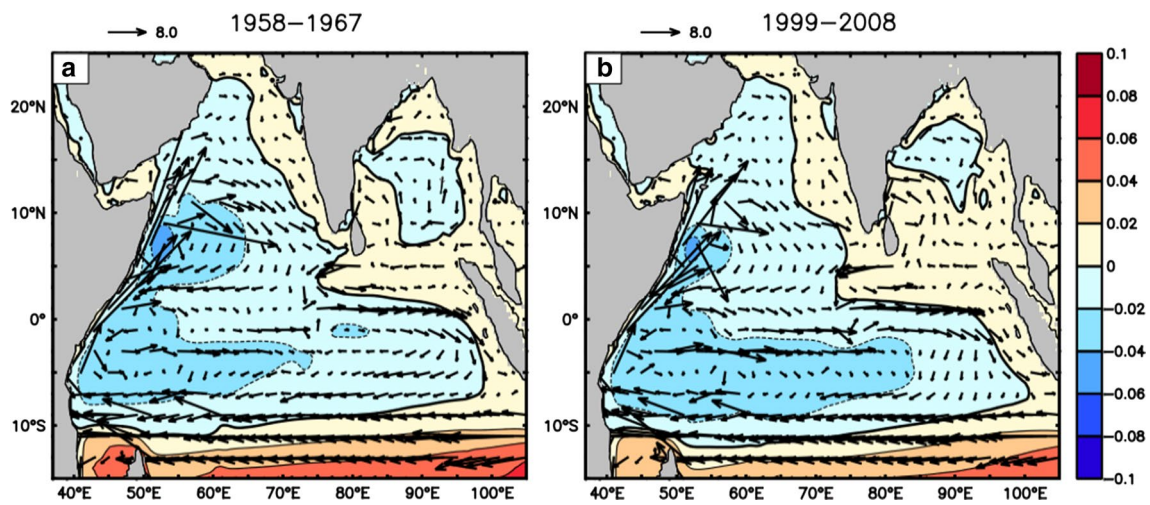

Fig. 8 Mean stream function (in Sv, *shaded*) and corresponding rotational component (10^4 m²/s, vectors) of upper 50 m volume fluxes for **a** 1958–1967, **b** 1999–2008 in CONTROL experiment
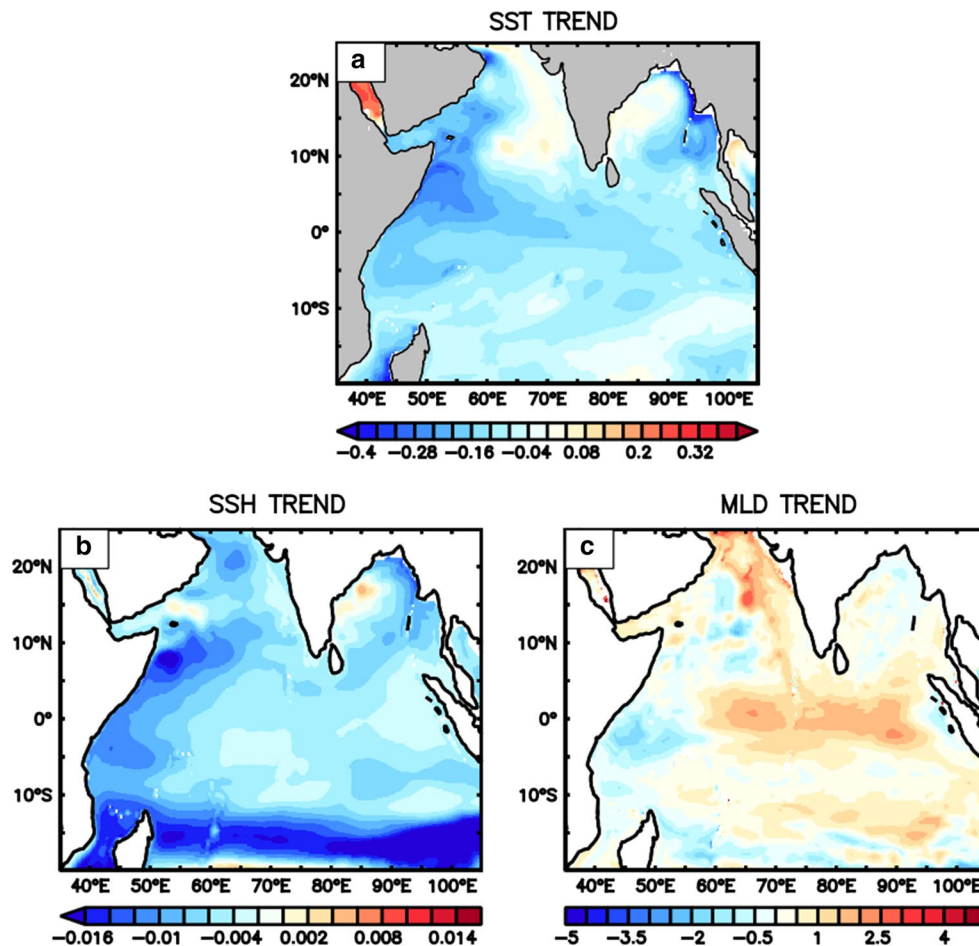
Fig. 9 **a** SST trends (°C/decade), **b** SSH trends (metre/decade), **c** MLD trend (metre/decade) in NHF_CLIM experiment

Figure 11 shows the vertical structure of temperature trend over TIO (zonal average from 50°E-100°E) in the three experiments. The observed vertical structure of TIO warming trend is simulated reasonably in CONTROL experiment. The tropical IO surface warming and subsurface cooling at thermocline level is reproduced by the model. The CLIM-PO experiment reproduced the surface warming and its deeper penetration similar to CONTROL, confirming that the surface warming is forced locally. But the magnitude of subsurface cooling has reduced considerably. The subsurface cooling is clearly evident in CLIM-IO experiment indicating that the subsurface cooling at thermocline level in TIO is contributed by variability in Pacific via ITF. Even in the absence of remote forcing from Pacific, the surface warming in the CLIM-PO experiment (north of 20°S) did not penetrate to deeper ocean. This suggests that both the Pacific remote forcing and the local forcing are jointly responsible for subsurface cooling observed in TIO.

At interannual timescales, thermocline depth anomalies associated with ENSO in the Pacific can be transmitted through the Indonesian region to the Indian Ocean where they propagate as Rossby waves (Cai et al. 2005). Alory et al. (2007) suggested that the subsurface cooling trend visible in IO along these off-equatorial Rossby wave pathways are associated with the signal of shoaling western Pacific thermocline transmitted to TIO in similar manner. Schwarzkopf and Böning (2011) showed evidence of this mechanism in an OGCM, with similar experiments. Several other model studies (Reason et al. 1996; Cai et al. 2008; Trenary and Han 2013) also identified the remote influence of Pacific wind forcing changes on IO decadal variability.

To see whether the forcing is via the modulation of Rossby wave propagation as proposed in these studies, we analyzed the thermocline depth anomalies along the Rossby wave pathway in southern TIO. Figure 12 shows the time-longitude section of thermocline depth anomalies (20° isotherm depth, averaged from 15°S–5°S) in CONTROL, CLIM–PO and CLIM-IO experiments. Anomalies are computed by subtracting CLIM output from each run. The westward propagating positive thermocline depth anomalies, which were dominant in the earlier decades, are replaced by negative anomalies in the recent decades. In the CLIM-PO

Fig. 10 **a** SST trends (°C/decade), **b** SSH trends (metre/decade), **c** MLD trend (metre/decade) in WIND_CLIM experiment
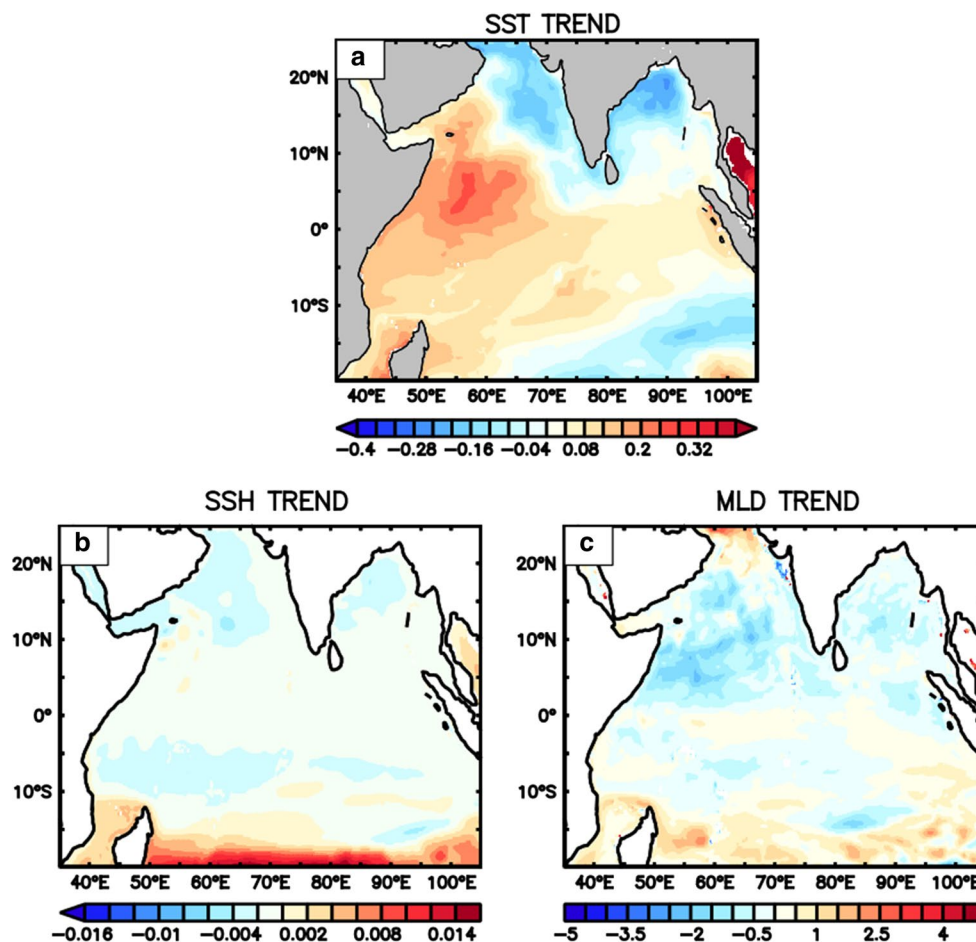
experiment, the westward propagating thermocline anomalies are of similar magnitude as in CONTROL, but the difference between the first half and later half of the study period evident in CONTROL, is not visible in CLIM-PO. This suggests that the long term changes in Rossby waves are not induced by local atmospheric forcing. In the CLIM-IO experiment, the thermocline depth anomalies are relatively weaker, but the reversal of sign in westward propagating thermocline depth anomalies in recent years is clearly visible. The thermocline shoaling and subsurface cooling in TIO are thus largely due to the transmission of shoaling thermocline signature from western Pacific to IO via ITF pathway, which propagates into interior IO by modulating the Rossby waves over southern TIO.

6 Summary and discussions

The changing surface circulation over TIO is studied using ocean reanalysis datasets and OGCM experiments. The large scale surface circulation features are strengthening in TIO in the recent decades. These circulation changes are mainly forced by large scale wind pattern changes and also

by geostrophic response of decreasing sea surface height in TRG region. The decreasing SSH/thermocline in TRG region is forced both by local wind changes and is amplified by the transmission of shoaling thermocline signal in the western Pacific via Indonesian archipelago through wave pathways.

The typical structure of the mean winds over the equatorial IO is a near linear gradient in zonal wind stress from south to north with almost zero winds at equator with no Ekman pumping, thereby equating Ekman drift and Sverdrup transport (Miyama et al. 2003). The wind trends indicate that this structure has undergone major changes, as westerly flow over both sides of equator has intensified. The mass convergence along the equator associated with the intensified westerly winds and the increase eastward currents along the equator can warm the central and eastern TIO. At the same time increasing divergence in the western equatorial IO can reduce SST in the west. The east–west gradient generated can further intensify the equatorial westerlies. The relative surface warming of the central equatorial IO drives winds towards the equatorial region, further enhancing equatorial westerlies. This mechanism can act as a positive feedback for SST warming in equatorial IO.

Fig. 11 Subsurface temperature trends (°C/decade, averaged from 50°E to 100°E) in **a** CONTROL, **b** CLIM-PO and **c** CLIM-IO experiments
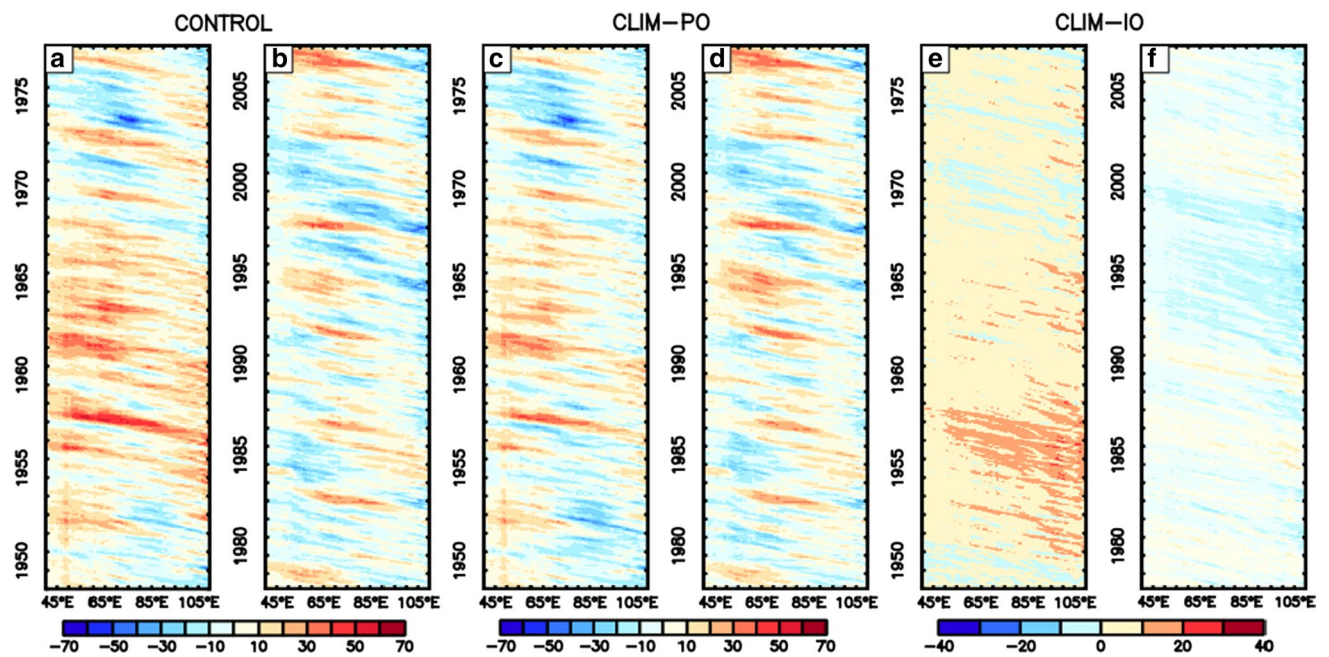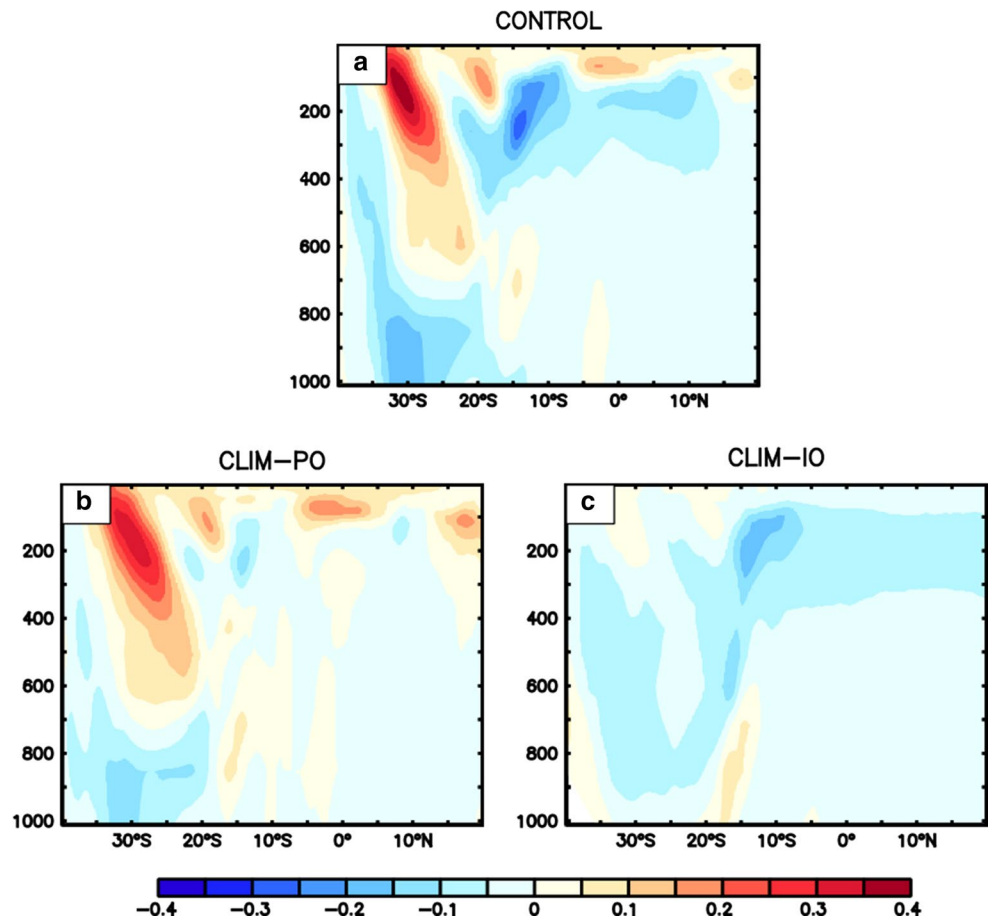

Fig. 12 Time longitude plot of 20° isotherm depth in southern TIO (averaged from 15°S to 5°S) in CONTROL (**a**, **b**), CLIM-PO (**c**, **d**), CLIM-IO (**e**, **f**)

The OGCM sensitivity experiments demonstrated that in the absence of wind induced circulation changes, the heat is accumulating in the western TIO, where ocean gains maximum heat. The experiment with no heat flux changes, but only wind induced responses showed cooling all over the basin, with maximum cooling over the west. This shows that only dynamic response cannot warm the ocean. The experiments suggest that strengthening of ocean circulation redistributes the excess heat received in west to the central and eastern TIO. The increasing SST in central TIO results in increased latent heat loss from the ocean (Rahul and Gnanaseelan 2013). The proposed mechanism explains the negative net heat flux trend over central TIO as the excess heat is received at western TIO which is redistributed to central and eastern parts by strengthening ocean circulation, increasing SST and latent heat loss from these region. This study strongly suggests that changing surface circulation features can significantly modulate the surface warming pattern of TIO. Model sensitivity experiments reveal that the subsurface cooling at thermocline level in TIO is contributed by variability in Pacific via Indonesian Through Flow whereas the surface warming trend is mainly induced by the changes in the local forcing. The study reveals that the long term changes in IO Rossby waves are not induced by local atmospheric forcing but are forced by Pacific. The thermocline shoaling in the west is amplified by the remote influence of Pacific via wave transmission through Indonesian archipelago.

References

Alory G, Meyers G (2009) Warming of the upper equatorial Indian Ocean and changes in the heat budget (1960–99). J Clim 22(1):93–113. doi:10.1175/2008JCLI2330.1

Alory G, Wijffels S, Meyers G (2007) Observed temperature trends in the Indian Ocean over 1960–1999 and associated mechanisms. Geophys Res Lett 34(2):L02606. doi:10.1029/2006GL028044

Balmaseda MA, Mogensen K, Weaver AT (2013) Evaluation of the ECMWF ocean reanalysis system ORAS4. Q J R Meteorol Soc 139(674):1132–1161. doi:10.1002/qj.2063

Barnett TP, Pierce DW, Achutarao KM, Gleckler PJ, Santer BD, Gregory JM, Washington WM (2005) Penetration of human-induced warming into the world's oceans. Science 309(5732):284–287. doi:10.1126/science.1112418

Cai W, Meyers G, Ge S (2005) Transmission of ENSO signal to the Indian Ocean. Geophys Res Lett 32(5):L05616. doi:10.1029/2004GL021736

Cai W, Cowan T, Dix M (2007) Anthropogenic aerosol forcing and the structure of temperature trends in the southern Indian Ocean. Geophys Res Lett 34(14):L14611. doi:10.1029/2007GL030380

Cai W, Sullivan A, Cowan T (2008) Shoaling of the off-equatorial south Indian Ocean thermocline: Is it driven by anthropogenic forcing? Geophys Res Lett 35(12):L12711. doi:10.1029/2008GL034174

Carton JA, Giese BS (2008) A reanalysis of ocean climate using simple ocean data assimilation (SODA). Mon Weather Rev 136(8):2999–3017. doi:10.1175/2007MWR1978.1

Chung CE, Ramanathan V (2006) Weakening of North Indian SST gradients and the monsoon rainfall in India and the Sahel. J Clim 19(10):2036–2045. doi:10.1175/JCLI3820.1

Deser C, Phillips AS, Alexander MA (2010) Twentieth century tropical sea surface temperature trends revisited. Geophys Res Lett 37(10):L10701. doi:10.1029/2010GL043321

Dong L, Zhou T (2014) The Indian Ocean sea surface temperature warming simulated by CMIP5 models during the twentieth century: competing forcing roles of GHGs and anthropogenic aerosols. J Clim 27(9):3348–3362. doi:10.1175/JCLI-D-13-00396.1

Dong L, Zhou T, Wu B (2013) Indian Ocean warming during 1958–2004 simulated by a climate system model and its mechanism. Clim Dyn 42(1–2):203–217. doi:10.1007/s00382-013-1722-z

Du Y, Xie S-P (2008) Role of atmospheric adjustments in the Tropical Indian Ocean warming during the 20th century in climate models. Geophys Res Lett 35(8):L08712. doi:10.1029/2008GL033631

Fox-Kemper B, Ferrari R, Hallberg R (2008) Parameterization of mixed layer eddies. Part I: theory and diagnosis. J Phys Oceanogr 38(6):1145–1165

Giannini A, Saravanan R, Chang P (2003) Oceanic forcing of Sahel rainfall on interannual to interdecadal time scales. Science 302(5647):1027–1030. doi:10.1126/science.1089357

Griffies SM, Hallberg RW (2000) Biharmonic Friction with a Smagorinsky-like viscosity for use in large-scale eddy-permitting ocean models. Mon Weather Rev 128(8):2935–2946. doi:10.1175/1520-0493(2000)128<2935:BFWASL>2.0.CO;2

Griffies SM, Harrison MJ, Pacanowski RC, Rosati A (2004) A technical guide to MOM4. GFDL Ocean Group Technical Report No. 5, p 337

Griffies SM et al (2005) Formulation of an ocean model for global climate simulations. Ocean Sci 2(3):165–246. doi:10.5194/osd-2-165-2005

Han W, Meehl GA, Hu A (2006) Interpretation of tropical thermocline cooling in the Indian and Pacific oceans during recent decades. Geophys Res Lett 33(23):L23615. doi:10.1029/2006GL027982

Han W et al (2010) Patterns of Indian Ocean sea-level change in a warming climate. Nat Geosci 3(8):546–550. doi:10.1038/ngeo901

Han W, Vialard J, McPhaden MJ, Lee T, Masumoto Y, Feng M, de Ruijter WPM (2014) Indian Ocean decadal variability: a review. Bull Am Meteorol Soc. doi:10.1175/BAMS-D-13-00028.1

Hoerling MP, Kumar A (2003) The perfect ocean for drought. Science 299(5607):691–694. doi:10.1126/science.1079053

Hoerling MP, Hurrell JW, Xu T, Bates GT, Phillips AS (2004) Twentieth century North Atlantic climate change. Part II: understanding the effect of Indian Ocean warming. Clim Dyn 23(3–4):391–405. doi:10.1007/s00382-004-0433-x

Ingleby B, Huddleston M, Breu FX, Guggenbichler S, Wollmann JC (2007) Quality control of ocean temperature and salinity profiles—historical and real-time data. J Mar Syst 65(1–4):158–175. doi:10.1016/j.jmarsys.2005.11.019

Kara AB, Rochford PA, Hurlburt HE (2000) An optimal definition for ocean mixed layer depth. J Geophys Res 105(C7):16803. doi:10.1029/2000JC900072

Large WG, Yeager SG (2008) The global climatology of an interannually varying air–sea flux data set. Clim Dyn 33(2–3):341–364. doi:10.1007/s00382-008-0441-3

Large WG, McWilliams JC, Doney SC (1994) Oceanic vertical mixing: a review and a model with a nonlocal boundary layer parameterization. Rev Geophys 32(4):363–403. doi:10.1029/94RG01872

Levitus S (2005) Warming of the world ocean, 1955–2003. Geophys Res Lett 32(2):L02604. doi:10.1029/2004GL021592

Levitus S, Antonov JI, Boyer TP, Locarnini RA, Garcia HE, Mishonov AV (2009) Global ocean heat content 1955–2008 in light of recently revealed instrumentation problems. Geophys Res Lett. doi:10.1029/2008GL037155

Li Q, Ren RC, Cai M, Wu GX (2012) Attribution of the summer warming since 1970s in Indian Ocean Basin to the inter-decadal change in the seasonal timing of El Niño decay phase. Geophys Res Lett. doi:10.1029/2012GL052150

Luo JJ, Sasaki W, Masumoto Y (2012) Indian Ocean warming modulates Pacific climate change. Proc Natl Acad Sci USA 109(46):18701–18706. doi:10.1073/pnas.1210239109

Lyman JM, Good SA, Gouretski VV, Ishii M, Johnson GC, Palmer MD, Smith DM, Willis JK (2010) Robust warming of the global upper ocean. Nature 465(7296):334–337. doi:10.1038/nature09043

Manizza M, Le Quéré C, Watson AJ, Buitenhuis ET (2005) Bio-optical feedbacks among phytoplankton, upper ocean physics and sea-ice in a global model. Geophys Res Lett 32(5):1–4. doi:10.1029/2004GL020778

Mishra V, Smoliak BV, Lettenmaier DP, Wallace JM (2012) A prominent pattern of year-to-year variability in Indian Summer Monsoon Rainfall. Proc Natl Acad Sci USA 109(19):7213–7217. doi:10.1073/pnas.1119150109

Miyama T, McCreary JP, Jensen TG, Loschnigg J, Godfrey S, Ishida A (2003) Structure and dynamics of the Indian-Ocean cross-equatorial cell. Deep Sea Res Part II Top Stud Oceanogr 50(12–13):2023–2047. doi:10.1016/S0967-0645(03)00044-4

Nidheesh AG, Lengaigne M, Vialard J, Unnikrishnan AS, Dayan H (2013) Decadal and long-term sea level variability in the tropical Indo-Pacific Ocean. Clim Dyn 41(2):381–402. doi:10.1007/s00382-012-1463-4

Rahul S, Gnanaseelan C (2013) Net heat flux over the Indian Ocean: trends, driving mechanisms, and uncertainties. IEEE Geosci Remote Sens Lett 10(4):776–780

Rao RR, Kumar MSG, Ravichandran M, Rao AR, Gopalakrishna VV, Thadathil P (2010a) Interannual variability of Kelvin wave propagation in the wave guides of the equatorial Indian Ocean, the coastal Bay of Bengal and the southeastern Arabian Sea during 1993–2006. Deep Sea Res Part I Oceanogr Res Pap 57(1):1–13. doi:10.1016/j.dsr.2009.10.008

Rao SA, Chaudhari HS, Pokhrel S, Goswami BN (2010b) Unusual Central Indian Drought of Summer Monsoon 2008: role of Southern Tropical Indian Ocean Warming. J Clim 23(19):5163–5174. doi:10.1175/2010JCLI3257.1

Rayner NA, Parker DE, Horton EB, Folland CK, Alexander LV, Rowell DP, Kent EC, Kaplan A (2003) Globally complete analyses of sea surface temperature, sea ice and night marine air temperature, 1871–2000. J Geophys Res 108:4407. doi:10.1029/2002JD002670

Reason CJC, Allan RJ, Lindesay JA (1996) Evidence for the influence of remote forcing on interdecadal variability in the southern Indian Ocean. J Geophys Res 101(C5):11867–11882

Roxy MK, Ritika K, Terray P, Masson S (2014) The curious case of Indian Ocean warming. J Clim 27(22):8501–8509. doi:10.1175/JCLI-D-14-00471.1

Schott FA, McCreary JP (2001) The monsoon circulation of the Indian Ocean. Prog Oceanogr 51(1):1–123. doi:10.1016/S0079-6611(01)00083-0

Schott FA, Xie S-P, McCreary JP (2009) Indian Ocean circulation and climate variability. Rev Geophys 47(1):RG1002. doi:10.1029/2007RG000245

Schwarzkopf FU, Böning CW (2011) Contribution of Pacific wind stress to multi-decadal variations in upper-ocean heat content

and sea level in the tropical south Indian Ocean. Geophys Res Lett 38(12):L12602. doi:10.1029/2011GL047651

Shenoi SSC, Saji PK, Almeida AM (1999) Near-surface circulation and kinetic energy in the Tropical Indian Ocean derived from Lagrangian drifters. J Mar Res 57(6):885–907. doi:10.1357/002224099321514088

Simmons HL, Jayne SR, Laurent LCS, Weaver AJ (2004) Tidally driven mixing in a numerical model of the ocean general circulation. Ocean Model 6(3–4):245–263. doi:10.1016/S1463-5003(03)00011-8

Sindhu B, Suresh I, Unnikrishnan AS, Bhatkar NV, Neetu S, Michael GS (2007) Improved bathymetric datasets for the shallow water. J Earth Syst Sci 116(3):261–274. doi:10.1007/s12040-007-0025-3

Smith TM, Reynolds RW, Peterson TC, Lawrimore J (2008) Improvements to NOAA's historical merged land-ocean surface temperature analysis (1880–2006). J Clim 21(10):2283–2296. doi:10.1175/2007JCLI2100.1

Sreenivas P, Gnanaseelan C, Prasad KVSR (2012) Influence of El Niño and Indian Ocean dipole on sea level variability in the Bay of Bengal. Glob Planet Change 80–81:215–225. doi:10.1016/j.gloplacha.2011.11.001

Swapna P, Krishnan R, Wallace JM (2013) Indian Ocean and monsoon coupled interactions in a warming environment. Clim Dyn. doi:10.1007/s00382-013-1787-8

Timmermann A, McGregor S, Jin F-F (2010) Wind effects on past and future regional sea level trends in the southern Indo-Pacific. J Clim 23(16):4429–4437. doi:10.1175/2010JCLI3519.1

Tokinaga H, Xie S-P, Deser C, Kosaka Y, Okumura YM (2012) Slowdown of the Walker circulation driven by tropical Indo-Pacific warming. Nature 491(7424):439–443. doi:10.1038/nature11576

Trenary LL, Han W (2008) Causes of decadal subsurface cooling in the Tropical Indian Ocean during 1961–2000. Geophys Res Lett 35(17):L17602. doi:10.1029/2008GL034687

Trenary L, Han W (2013) Local and remote forcing of decadal sea level and thermocline depth variability in the south Indian Ocean. J Geophys Res Ocean 118(1):381–398. doi:10.1029/2012JC008317

Unnikrishnan AS, Shankar D (2007) Are sea-level-rise trends along the coasts of the north Indian Ocean consistent with global estimates? Glob Planet Change 57(3–4):301–307. doi:10.1016/j.gloplacha.2006.11.029

Vargas-Hernandez JM, Wijffels SE, Meyers G, Belo do Couto A, Holbrook NJ (2015a) Decadal characterization of Indo-Pacific Ocean subsurface temperature modes in SODA reanalysis. J Clim 28(15):6113–6132. doi:10.1175/JCLI-D-14-00700.1

Vargas-Hernandez JM, Wijffels S, Meyers G, Holbrook NJ (2015b) Slow westward movement of salinity anomalies across the tropical south Indian Ocean. J Geophys Res. doi:10.1002/2015JC010933

Watterson IG (2001) Decomposition of global ocean currents using a simple iterative method. J Atmos Ocean Technol 18(4):691–703. doi:10.1175/1520-0426(2001)018<0691:DOGOCU>2.0.CO;2

Williams AP, Funk C (2011) A westward extension of the warm pool leads to a westward extension of the Walker circulation, drying eastern Africa. Clim Dyn 37(11–12):2417–2435. doi:10.1007/s00382-010-0984-y

Xie S-P, Deser C, Vecchi GA, Ma J, Teng H, Wittenberg AT (2010) Global warming pattern formation: sea surface temperature and rainfall. J Clim 23(4):966–986. doi:10.1175/2009JCLI3329.1